Applied Computing and Geosciences 27 (2025) 100271

Contents lists available at ScienceDirect

Applied Computing and Geosciences

journal homepage: www.sciencedirect.com/journal/applied-computing-and-geosciences

SRT-Ai: Identifying seismic reflection terminations using deep learning

Waleed M. AlGharbi [a,*], Rebecca E. Bell [a], Cédric M. John [b]

[a] Department of Earth Science and Engineering, Imperial College London, South Kensington Campus, London, SW7 2AZ, United Kingdom
[b] Digital Environment Research Institute, Queen Mary University of London, New Rd, London, E1 1HH, United Kingdom

ARTICLE INFO

Keywords:
Sequence stratigraphy
Seismic terminations
Synthetic
Deep learning
Classification

ABSTRACT

Seismic stratigraphy entails a regional scanning (reconnaissance) of seismic data to identify and annotate seismic reflection terminations. To identify these terminations in modern 3D seismic datasets, interpreters have to examine thousands of inlines and crosslines, which is a time-consuming process. Furthermore, accurate identification of these features relies heavily on human visual observation along with individual expertise.

A growing number of studies have shown promising results applying machine learning techniques to identify geological features from seismic data such as salt bodies and faults. However, the identification of seismic reflection terminations has not received the same level of interest and remains a manual process. One of the barriers to utilizing machine learning techniques in seismic interpretation is the lack of "labelled" data. In this study, we evaluate the ability of deep learning Convolutional Neural Networks (CNN) trained on synthetic seismic images to identify seismic reflection terminations.

A dataset comprising 160 000 synthetic seismic images that represent conformable and four types of seismic reflection terminations (truncation, toplap, onlap, and downlap) were created using geometric geological modelling and 1D convolution seismic modelling. The dataset was then split into two classes ("Contains Termination" and "No Termination"). A new CNN model architecture named "Seismic Reflection Terminations Attribute (SRT-Ai)" was trained on 80 % of the synthetic seismic dataset. SRT-Ai predicted the test set (remaining 20 %) with an accuracy and precision of 99.9 %. To test its generalization, SRT-Ai was also evaluated on real seismic images, achieving 91 % accuracy and 96 % precision against published interpretations used as reference labels. Qualitative analysis of predictions along seismic sections shows a strong correspondence between the model predictions and manual regional interpretations.

SRT-Ai is proposed as a screening tool that will assist seismic interpreters with the identification of major seismic terminations, minimise seismic interpretation uncertainties, reduce the time taken for seismic reconnaissance, and limit the reliance on human visual observation at the early stage of seismic interpretation process.

1. Introduction

In 1921, a seismic reflection profile started the revolution of reflection seismology applications in exploration (Dragoset, 2005). Since then, seismic data has become an essential and dominant tool in characterizing, mapping, and modelling the subsurface (Telford et al., 1990). Seismic data, especially 3D seismic data, is an excellent tool for mapping subsurface geometries to investigate tectonic settings, depositional stacking patterns, and stratal terminations with good lateral and vertical coverage. Today, 3D seismic data is an integral part of most subsurface sedimentary basins' studies (Chopra and Marfurt, 2012).

Legacy and newly acquired high fold seismic data are currently playing a major role in environment protection and energy transition plans (Han et al., 2021). Utilizing state of the art technologies to drill fewer wells with higher success rate can lower the environmental impact of hydrocarbon exploration. In addition, reducing carbon concentration in the atmosphere through carbon sequestration requires detailed subsurface characterization to understand the seal and reservoir properties as well as delineating reservoirs storage capacity (Riding and Rochelle, 2009). Moreover, monitoring 4D seismic data through time helps to de-risk and mitigate any geohazards associated with CO_2 leakage. Other seismic applications in energy transition include identifying potential locations for offshore wind turbines and geothermal sweet spots (Gold et al., 2022).

This article is part of a special issue entitled: Planetary Mapping published in Applied Computing and Geosciences.

* Corresponding author.
E-mail address: w.algharbi21@imperial.ac.uk (W.M. AlGharbi).

https://doi.org/10.1016/j.acags.2025.100271
Received 29 October 2024; Received in revised form 24 July 2025; Accepted 24 July 2025
Available online 26 July 2025

Utilizing seismic data to image and interpret the subsurface was revolutionised in the 1970s with the introduction of seismic stratigraphy. It involves the use of sequence stratigraphy concepts to interpret seismic data with the assumption that every reflection in seismic data represent a chronostratigraphic timeline (Eberli et al., 2022; Vail and Mitchum Jr, 1977). Seismic stratigraphy relies on accurate identification of seismic reflection terminations to map stratigraphic architectures, depositional environments, and lithofacies distribution (Catuneanu et al., 2009; Christie-Blick et al., 1990; Summerhayes, 1986; Vail and Mitchum Jr, 1977) (Fig. 1). However, most current seismic interpretation packages focus on automating the process of picking reflections to generate continuous and smooth maps (Posamentier et al., 2022). Marking reflection terminations or annotating features like clinoforms' lapouts, erosional surfaces, and basin limits, despite their importance in seismic stratigraphy analysis, are still missing in most interpretation packages.

During the last decade, Artificial Intelligence (AI) and machine learning have played a key role in advancing the automation of seismic interpretation. The parallel progression of powerful GPU architectures and deep learning algorithms capable of handling big and complex data contributed to the recent advancement in deep learning application in many fields, including seismic interpretation. Recent studies show promising results using machine learning to pick seismic horizons, predict seismic facies, and identify geological features such as salt bodies and faults (e.g., Gu et al., 2023; Kaur et al., 2023; Tschannen et al., 2020; Waldeland et al., 2018; Wrona et al., 2021; Zhang et al., 2018; Zheng et al., 2019). Identification of seismic reflection terminations using deep learning is still underexplored and remains a conventional and manual process.

The main challenge that delays the adaptation of machine learning applications in seismic interpretation is the lack of "labelled" data (Gao et al., 2023). Labelling seismic data is time consuming and can introduce interpretation bias. In this study, we are evaluating the ability of deep learning neural networks to identify seismic reflection terminations using synthetic seismic dataset, without the need for human "labelling". Synthetic seismic have been previously effectively employed as ground truth labels for training and validating machine learning models in various seismic interpretation applications (e.g. Vizeu et al., 2022; Wu et al., 2020). By generating synthetic seismic dataset instead of using real seismic for training, we avoid adding interpretation bias and reduce the time required for manual labelling.

We trained a deep learning Convolutional Neural Networks (CNN) model for binary classification to identify termination and non-termination geometries in seismic data. The training data are synthetic seismic responses generated through geological modelling with two classes: "Contains Termination" and "No Termination". This formulation enabled the model to learn from labelled examples and classify seismic geometries accordingly.

This study introduces a new AI screening tool (SRT-Ai) that can identify and highlight seismic reflection terminations in seismic quickly and accurately with minimal human intervention. This tool is designed to help seismic interpreters identify key seismic reflection terminations which can be then interpreted using various interpretation packages to build stratigraphic frameworks more quickly and effectively.

2. Methodology

2.1. *Generating geological models*

Five groups of geological models represented by different stratal geometries were created: conformable models containing no termination, and unconformable models containing one of four stratigraphic termination types (truncation, toplap, onlap, and downlap) (Fig. 2). To create these models, we used bruges (Hall et al., 2022), a modelling library focusing on wedge models.

There are six parameters that control geological models in bruges (depth, width, strat, thickness, mode, and conformance) (Table 1):

Depth is the size of the y-axis in pixel index units, specifying the vertical dimensions of the model. It typically includes the top thickness, wedge thickness, and base thickness in a tuple. A relatively larger value (30 pixel units) was assigned to the top thickness of the terminated models compared to the conformable models (10 pixel units) to avoid having the terminations at or very close to the top edge of the windows. Width is the size of the x-axis in pixel index units, defining the horizontal dimensions of the model. Unlike the depth parameter, the tuple numbers in width represent left extension, wedge, and right extension. Since reflectors terminate only in the wedged (middle) section, the total length of the x-axis (200 pixel units) was assigned to the middle-section with zero values to the side sections, where the models extend beyond termination points. The resulted geological models are unitless arrays with (200 pixels $\times$ 100 pixels) image size.

Strat is the parameter that defines the stratigraphy (rock layers) above, within, and below the wedge. While depth parameter controls the overall thickness of the wedge as well as the thickness of the upper and lower bounding layers, strat determines both the number of layers and their individual thicknesses within the wedge and its bounding layers. To simulate the synthetic stratigraphic sequences, we implemented a Python loop that generates a column of rock layers, up to a maximum of eight units. Each layer is randomly assigned a rock type that will be assigned an acoustic impedance value. This approach allows for the creation of varied yet controlled stratigraphic patterns.

Thickness specifies the variation in thickness across the wedge. Although the name "thickness" might be misleading, this parameter represents how sediment thickness changes across the entire wedge model, as determined by the ratio between the values at the lateral ends of the layers. These values are given as percentages, where 1.0 means 100 % thickness (full thickness) and 0.0 means the layer completely pinches out.

Mode determines how the wedge shape changes across the model. Two modes were used in building the geological models: linear and

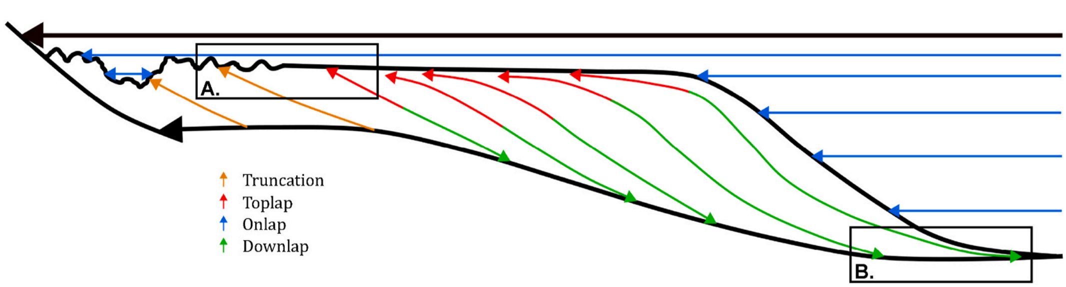

Fig. 1. A sequence stratigraphy diagram showing different types of stratigraphic terminations (after Vail et al., 1977). Truncation is an erosional surface indicating a removal of depositional strata along an unconformity. Toplap is an up-dip termination of tilted reflectors against relatively horizontal layer. Onlap is a termination of relatively horizontal reflectors against a tilted older depositional surface. Downlap is a down-dip termination of tilted depositional surface against a relatively horizontal surface.

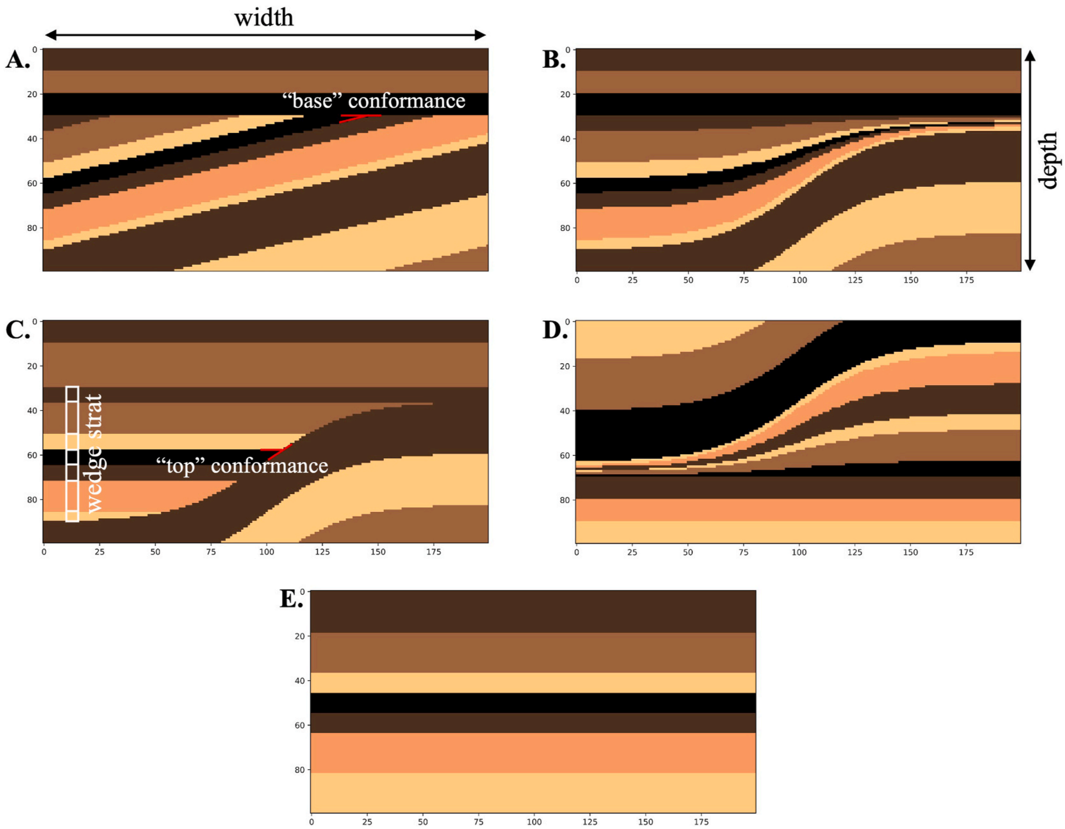

Fig. 2. Examples of base geometries for the five geological model groups, with main geometrical parameters annotated: (A) Truncation, (B) Toplap, (C) Onlap, (D) Downlap, and (E) Conformable.

Table 1
Six parameters control the size and shape of geological models.

		Geological Models				
		Truncation	Toplap	Onlap	Downlap	Conformable
Parameters	**depth** (top thickness, wedge thickness, base thickness)	(30, 60, 10)	(30, 60, 10)	(30, 60, 10)	v. flip (30, 60, 10)	(10, 80, 10)
	width (left extension, wedge length, right extension)	(0, 200, 0)	(0, 200, 0)	(0, 200, 0)	(0, 200, 0)	(0, 200, 0)
	strat (number of layers)	random (1–8)	random (1–8)	random (1–8)	random (1–8)	random (1–8)
	thickness (left thickness %, right thickness range %)	(1.0, 0.0–0.5)	(1.0, 0.0–0.4)	(1.0, 0.0–0.5)	(1.0, 0.0–0.4)	(1.0, 0.9–1.0)
	mode	linear	sigmoid	sigmoid	sigmoid	linear
	conformance	base	none	top	none	none

sigmoid. Sigmoid is the expected regional shape for clinoforms and basin limits (Fig. 2-B, 2-C, and 2-D), whereas linear was used for conformable and angular truncation models (Fig. 2-A and 2-E). Conformance dictates the termination direction. A "none" conformance is for models without terminations (e.g. conformable), "top" conformance is for top layers terminating against the lower layer (e.g. onlap), and "base" conformance is for base layers terminating against the upper layer (e.g. truncation). A "none" conformance was also used for toplaps and downlaps to maintain a gradual thinning of the terminated layers toward the termination point, where the layers will be too thin to be resolved seismically.

2.2. Geological models to synthetic seismic

Seismic forward modelling is the numerical computation of seismic responses to geological models, that attempts to simulate real subsurface seismic data (Hart and Chen, 2004; Krebes, 2004). In this study, the generated geological models were used as the base geometrical models to create synthetic seismic images using 1D convolution seismic modelling. A summary for the seismic forward modelling steps that were used to generate the synthetic seismic dataset is in Fig. 3. The first step in creating the synthetic seismic dataset from geological model is to fill the layers with acoustic impedance values. Acoustic impedance (Z) is the product of velocity and density. To calculate a set of possible acoustic impedance values, ranges of velocities (2000–6000 m/s) and densities (1.6–2.9 gm/cm^3) were used that represent the full range of sedimentary rock properties (Gregory, 1977; Kearey et al., 2002).

Reflection coefficients were then calculated at the interfaces between layers. For normal incidence, the reflection coefficient (R) is the difference in acoustic impedance of overlying layers over the sum of acoustic impedance of the same layers at the interface:

$$\textit{reflection coefficient } (R) = \frac{Z_{layer2} - Z_{layer1}}{Z_{layer2} + Z_{layer1}}$$

If the two layers have the same acoustic impedance there will be no reflection at the geological interface and it will appear that there is a single thick layer without a reflection in between.

The next step is to convolve the reflection coefficient with a wavelet to obtain synthetic seismic images. Choosing a wavelet with a suitable frequency that can resolve most of the layers and their termination

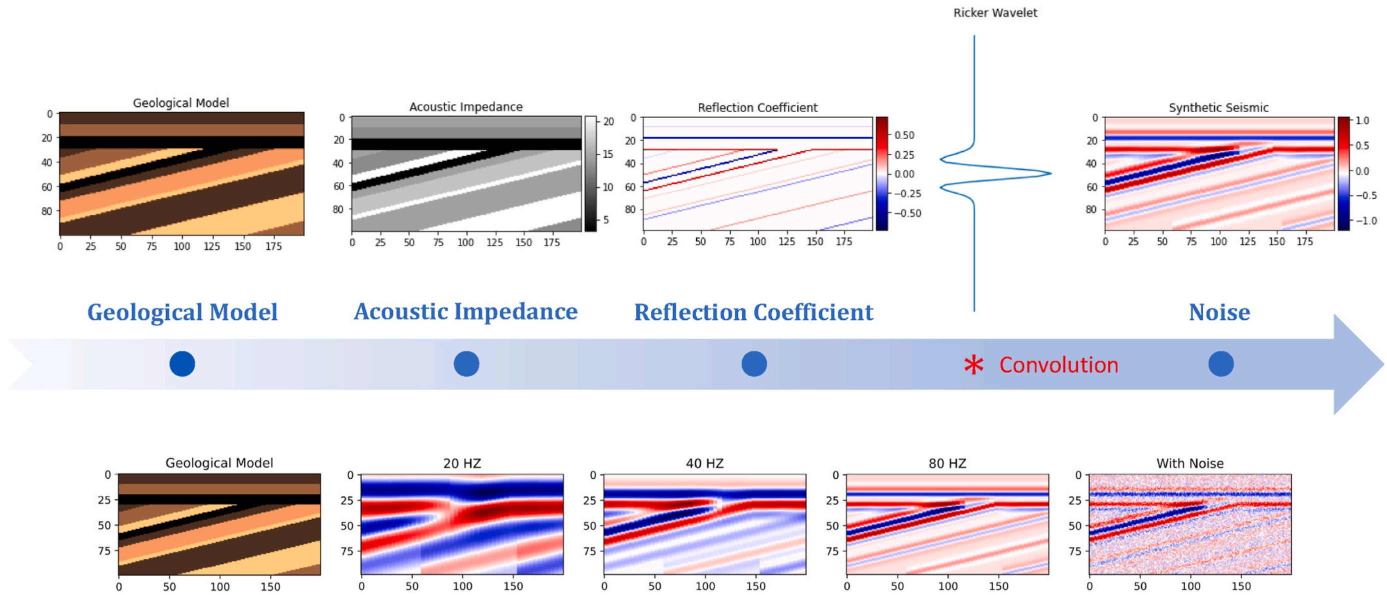

Fig. 3. Seismic forward modelling workflow. Three frequencies (20, 40, and 80 Hz) show different synthetic seismic resolutions.

points is crucial. A zero-phase Ricker wavelet with 80 Hz dominant frequency, 98 ms total length, and 1 ms sampling rate was used to resolve the layers in the geological models with peak amplitudes corresponding to increasing acoustic impedance (positive reflection coefficient). The Ricker wavelet provides the closest approximation of seismic signals both empirically and theoretically (Gholamy and Kreinovich, 2014; Ricker, 1953). This 80 Hz ricker wavelet was chosen in an attempt to generate a realistic synthetic seismic dataset given the thickness of the units in the geological models (Fig. 3). The chosen wavelet was then convolved with the reflection coefficients to build normal incidence synthetic seismic dataset (Russell, 1988):

$$synthetic\ seismic = wavelet * R$$

The final step in the workflow was to add random noise to the synthetic data. The added noise has a log-normal distribution with different intensity thus generating a dataset with a range of signal-to-noise ratios.

2.3. Data splitting and augmentation

Identifying seismic reflection terminations such as erosional truncation and toplap as different classes is challenging due to their similar geometries, with even human annotators struggling without a clear regional context. The resulting ambiguity limited the model's performance and caused instability during training, as it oscillated between the two classes. We opted to combine all termination types into a single class “Contains Terminations” for this study, with the intention of exploring multiclass approaches in future work (more discussion in section 4.1). Thus, synthetic data were grouped into two broad classes: “Contains Termination” and “No Termination”. The “Contains Termination” class comprises 80 000 models: 20 000 truncation, 20 000 toplap, 20 000 onlap, and 20 000 downlap models. The “No Termination” class comprises 60 000 conformable and an additional 20 000 labelled as conformable with lateral amplitude changes. In some geological scenarios, such as lateral changes in lithology or rock properties, the seismic response may show a "fadeout" termination effect, which can be mis-predicted as a stratigraphic termination. To address this ambiguity, we introduced the conformable models with lateral amplitude changes. These were constructed using configurations similar to onlap models, but with a reduced thickness range to (1.0, 0.7–0.9).

The generated synthetic seismic dataset was split into training, testing, and validation sets (Géron, 2019). The split was (80/20 % train/test set) and the training set was further split (80/20 % train/-validation set). This yielded 102 400 training instances, 25 600 validation instances, and 32 000 testing instances. Offline augmentation was then applied to the training dataset and added to the final training data set, which doubled the training instances to 204 800. This augmentation includes horizontal flipping, rotation ($\pm 10^{\circ}$ to maintain the overall geological representation of the models after augmentation), and zooming (50 % height and 20 % width factors).

2.4. Neural network architecture and training

Convolution Neural Networks (CNN) are a family of deep learning architectures that have been proven adept at identifying, mapping, and extracting visual features from images. This includes geological features such as faults, horizons, and salt bodies (Di et al., 2018; Wrona et al., 2021). LeCun et al. (1998) introduced CNN as a “specialized neural network architecture which incorporates knowledge about the invariances of 2D shapes by using local connection patterns and by imposing constrains on the weights”. CNN architectures are structured in a way that allow them to learn spatial hierarchies of features automatically to minimise the difference between outputs and labels through a backpropagation optimization process using a network of multiple layers.

It is common practice in classification problems to build CNNs that have multiple convolutional layers, each with an activation function that decides the status of each node in the network (Waldeland et al., 2018). Convolutional layers are the feature extraction layers where the network learns to identify and extract key patterns such as edges and shapes from the input data through mathematical convolutions. Each of these convolutional layers is followed by a pooling operation to downsample or subsample the feature maps. Pooling are regularization layers that reduce the resolution and dimensionality of the feature maps without learnable parameters, which helps in reducing the computational cost and minimizing overfitting. Another layer that helps in minimizing overfitting is dropout (Srivastava et al., 2014), randomly dropping a percentage of the nodes from each layer at every iteration. After the series of convolutional groups, the network ends with a fully connected “flattening” layer, a linear transformation operation that transform the output feature maps from the last convolutional layer to a one-dimension vector, and finally a classifier.

Most deep learning architectures require significant memory and computational resources due to their complexity and large number of parameters. In this study, we explored a simpler architecture to determine the minimum model complexity necessary to effectively address the binary problem we face. This approach allows us to balance performance with resource efficiency, making the solution more accessible and practical for environments with limited computational power. Our custom CNN architecture, which is named "SRT-Ai" for "Seismic Reflection Terminations Attribute" (Fig. 4), has three layers of 2D convolution. The first convolution layer has 16 filters with (15 x 15) kernel size. The second convolutional layer has 32 filters with (9 x 9) kernel size. Finally, the third layer has 64 filters with (3 x 3) kernel size. Each of these convolutional layers has a ReLU activation function (Nair and Hinton, 2010) followed by maxpooling. Maxpooling layers are down sampling mathematical operation layers that calculates the maximum value for the patches in the feature maps (Scherer et al., 2010). Maxpooling was chosen over other pooling types such as average pooling, global pooling, or mixed pooling to preserve the most prominent features. After several tests and iterations, 50 % dropout layer was used immediately after the flattening layer. The final step in the CNN is a softmax classifier, predicting the probabilities for each class.

A batch size of 128 was selected as it helped stabilise the learning curve and gives better performance. The selected loss function and optimizer were categorical-crossentropy and Adam respectively with early stopping triggered after 20 epochs of stagnant validation loss.

2.5. Model validation using real seismic

After the neural network was trained and tested on synthetic seismic images, a full 2D seismic section and several sliced 2D windows from a 3D seismic survey were used to test the model performance on real seismic images. Demeter, which is an open-source 3D seismic survey from northwestern Australia (Fig. 5), was used for the testing. This survey was selected because it has good signal to noise ratio with clear stratigraphic termination features, including examples of erosional truncation, onlap, downlap, toplap and conformable reflections. The Demeter covers 3590 km^2 with 133 nominal fold number. It was acquired in 2004, processed and made available for interpretation in 2005 (Bennett and Bussell, 2006). Based on data analysis and a review of multiple published interpretations (Anell and Wallace, 2020; Bennett and Bussell, 2006; Geoscience Australia, 2023; Hull and Griffiths, 2002), 100 seismic examples were extracted along different inlines (dip direction). The examples were evenly distributed among five categories: 20 truncation, 20 toplap, 20 onlap, 20 downlap, and 20 conformable (Fig. A.1). Each example measured 200 common depth points by 100 ms. This window size was chosen to be as small as possible while still capturing a single type of stratigraphic termination. In all cases, conformable continuous layers were expected to occupy at least part of each example.

To predict the presence of terminations with SRT-Ai on a full 2D seismic section and enable the spatial localization of stratigraphic terminations, seismic sections were divided into overlapping patches using a sliding window approach. A custom function was applied to extract patches with a fixed window size of (200 pixels × 99 pixels) sliding in a horizontal stride of ten and a vertical stride of three. Predictions for each patch were reshaped to a 2D map reflecting the layout of the sliding windows. For this binary classification task, the probability of the positive class was extracted and mapped with dimensions corresponding to the number of extracted windows in each spatial direction.

To visualize these predictions on the original seismic scale, a resampling step was performed. A dedicated function was used to interpolate the lower-resolution prediction map to the full resolution of the original seismic section. This was achieved by computing the scaling factors between the prediction grid and the seismic section dimensions, followed by interpolation. This resulted in about 50 000 predictions located at the centre of each sliding window averaging 660 samples per pixel with lower sampling rate at the edges of the section. The resampled prediction map retained the spatial alignment with the seismic data and enabled an overlay of classification results on the original section for interpretation and quality assessment (Fig. A.2).

3. Results

3.1. Synthetic seismic dataset

Each image in the generated synthetic seismic dataset has a different number of layers that vary in geometry, thickness, and reflectivity with a wide range of signal-to-noise ratios (Fig. 6). If we compare Fig. 6-A and 6-B they are both in the "No Termination" class with conformable geometry. However, (6-A) has more reflections with stronger amplitude, and the reflections are slightly tilted.

Since the process of assigning acoustic impedance to each layer was randomized, some scenarios resulted in very small differences in acoustic impedance between adjacent layers close to the termination point. This yielded weak or even zero reflectivity values (e.g. Fig. 6-E and 6-G). The noise level of the generated synthetic seismic also varied from high (e.g. Fig. 6-D and 6-G) to low (e.g. Fig. 6-B and 6-F).

3.2. Performance evaluation

The training curves (Fig. 7-A) show that the model converged within

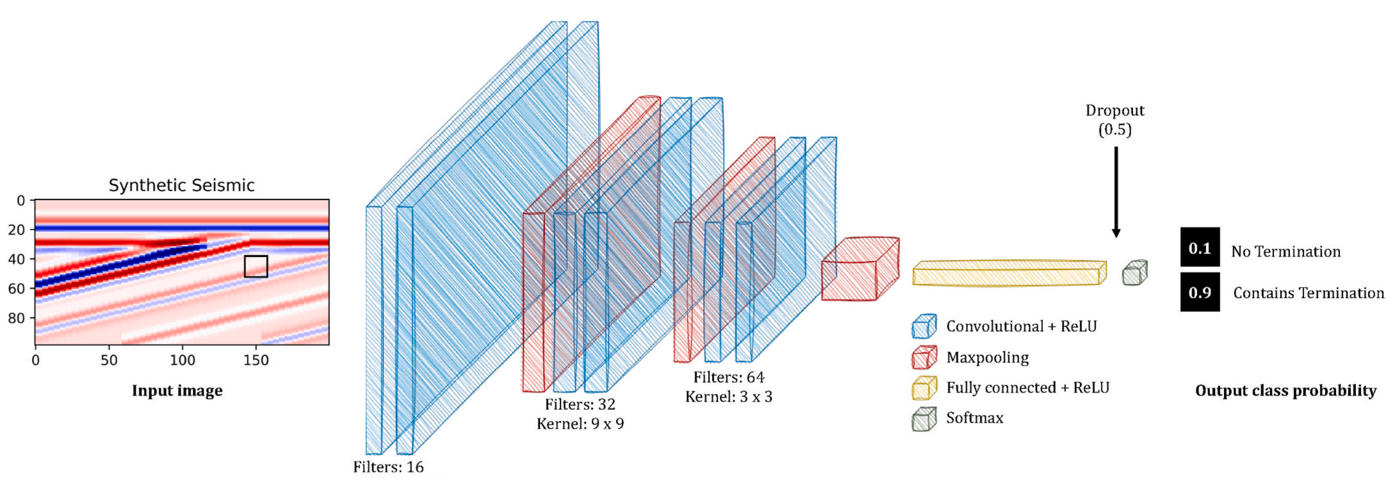

Fig. 4. The architecture of the Convolutional Neural Networks (CNN) used in the study.

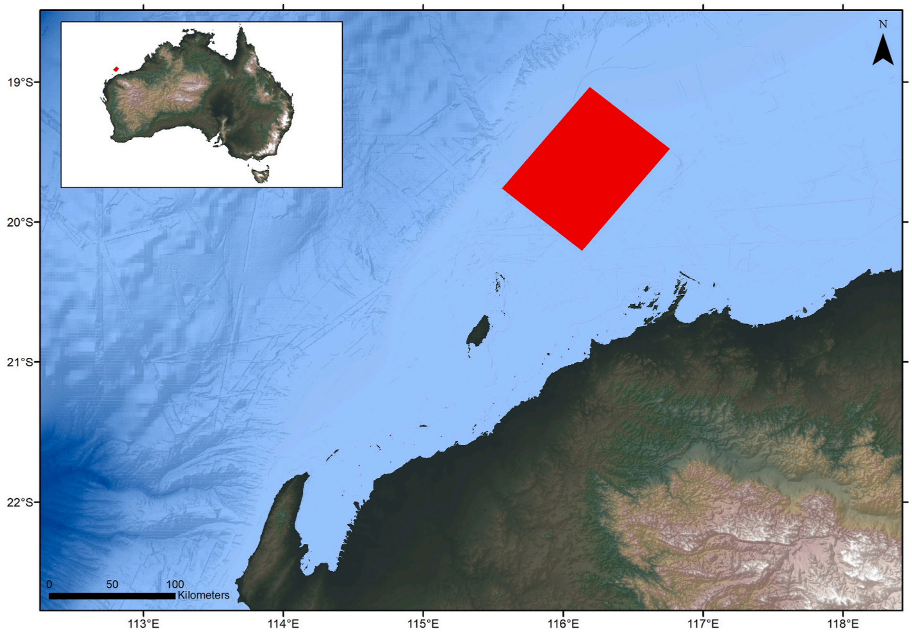

Fig. 5. Location map of the 3D seismic survey (red rectangle) used for testing the CNN. (For interpretation of the references to colour in this figure legend, the reader is referred to the Web version of this article.)

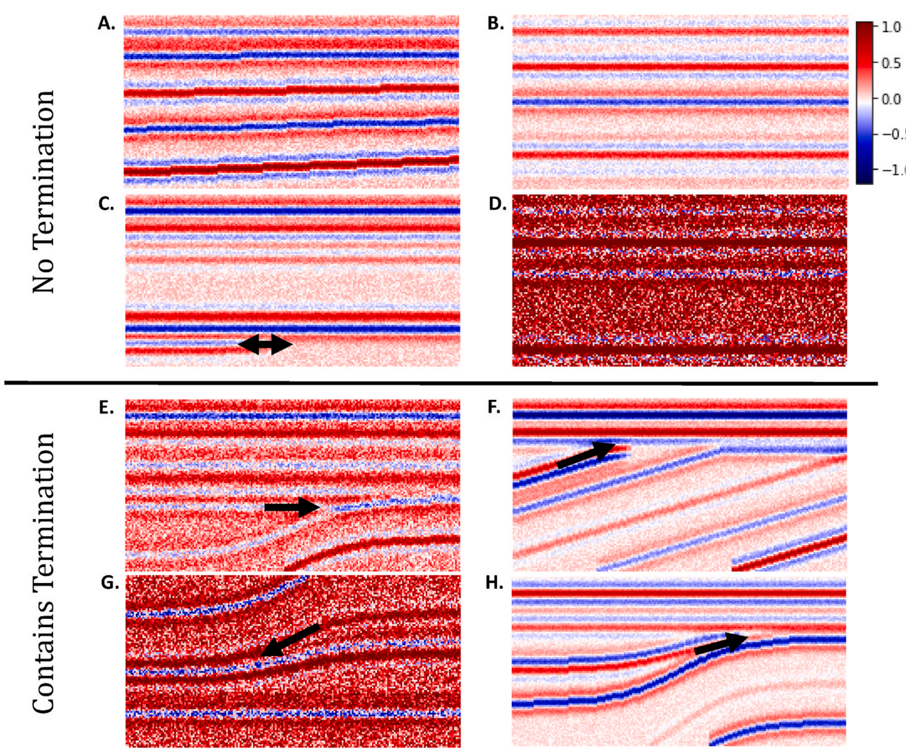

Fig. 6. Examples from the synthetic seismic dataset. The "No Termination" class has mainly continuous conformable layers, with some examples of laterally fading-out reflections to emulate the later change in rock properties (C). The double ended arrow in (C) shows the location of the lateral change in amplitude, whereas the other arrows show the direction of the terminations with the arrows' tips pointing the location of terminations.

10–20 epochs, with a lower validation loss than the training loss. This is expected as the augmentation was applied only on the training dataset. The results of testing SRT-Ai on unseen synthetic seismic dataset yielded 99.9 % in both accuracy and precision. The trained CNN correctly predicted all the "No Termination" classes and most of the "Contains Termination" of the synthetic test set. It missed only 13 out of 15 930 (0.08 %) samples from the "Contains Termination" class (Fig. 7-B). When applied to real seismic images, despite it being more complex, the accuracy and precision scores were still over 90 % (Table 2). The network performed well on predicting terminations in the real seismic testing dataset with 91 % accuracy, 96 % precision, 88 % recall, and 92 % f1-score. There were only 7 mis-predicted samples from the "Contains Termination" class (11.67 %) and 2 (5 %) from the "No Termination" class, out of 100 samples (Fig. 7-C).

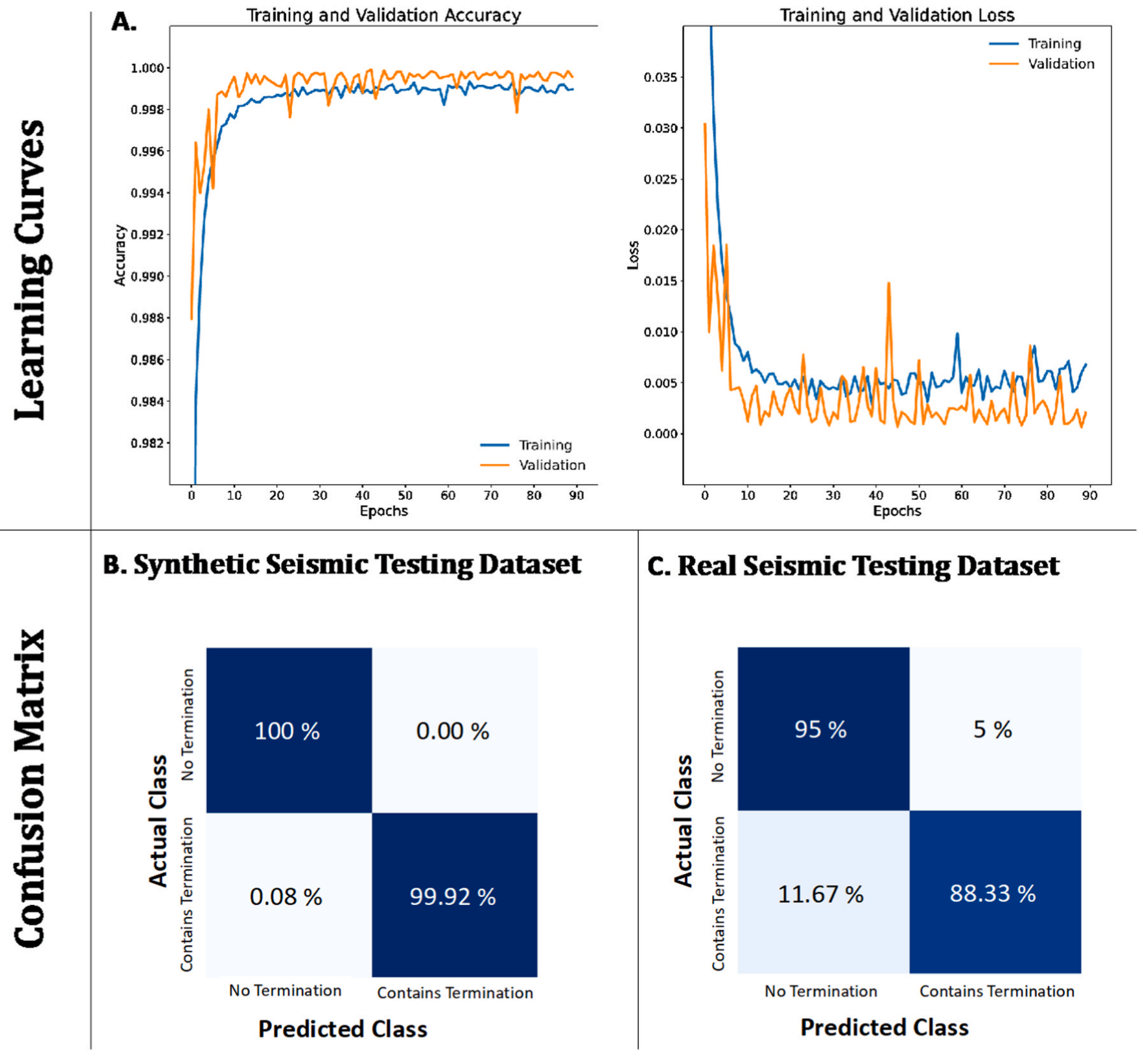

Fig. 7. The learning curves and predictions confusion matrixes.

Table 2
Summary of SRT-Ai performance.

		Performance							
		On Synthetic Seismic Testing Dataset				On Real Seismic Testing Dataset			
		Accuracy	*Precision*	*Recall*	*f1-score*	*Accuracy*	*Precision*	*Recall*	*f1-score*
Classes	No Termination	99.9 %	99.9 %	100 %	99.9 %	91 %	84 %	95 %	89 %
	Contains Termination	99.9 %	100 %	99.9 %	99.9 %	91 %	96 %	88 %	92 %

3.3. Applying SRT-Ai to real seismic

A dip-direction full 2D seismic section from the Demeter 3D seismic survey (Fig. 8-A) was used as a testing example to visually (qualitatively) evaluate the performance of SRT-Ai as an aid to seismic interpreters. This section was selected because an initial manual interpretation revealed that it has all the geological features that we are trying to identify using deep learning: toplaps, onlaps, and downlaps associated with multiple clinoforms as well as an angular unconformity with clear truncations. In addition, the section has some faults and reworked sediment (debris flow) geometries (Fig. 8-B). When SRT-Ai was deployed on the seismic section, most of these geological features were highlighted with high probability of containing termination (Fig. 8-C).

4. Discussion

4.1. The challenges of seismic termination classification with deep learning

During the progress of this research, we were faced with three main challenges centred around prediction optimizations: The first challenge was that identification of the type of seismic reflection termination (e.g. truncation, toplap, onlap etc.) at the scale of the data used in our classification window proved to be impracticable. There are geological scenarios where different stratigraphic termination types that represent different depositional and/or tectonic settings have similar, or identical geometry in seismic sections. Fig. 1-box (A) is one of the scenarios where two different stratigraphic termination types have the same geometry. The red arrow is a toplap, where tilted layers terminate against a

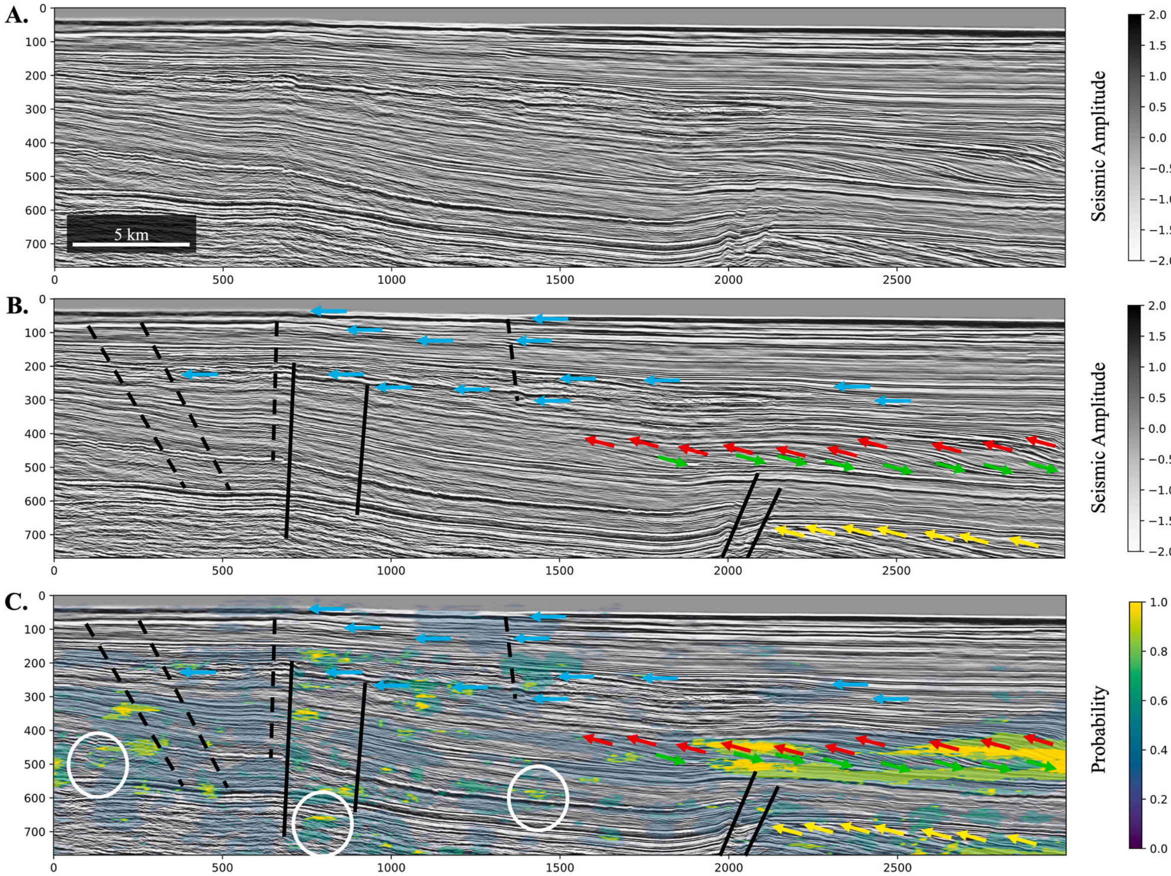

Fig. 8. (A) An uninterpreted seismic section. (B) The same seismic section with manual interpretation and annotations for stratigraphic terminations and faults [light blue arrows are for onlaps, yellow arrows are for truncations, green arrows are for downlaps, and red arrows are for toplaps. The solid black lines are for faults with high confidence and dashed once are possible faults]. (C) The annotations are overlaying the SRT-Ai attribute. There is a strong correlation between the annotations and attribute probability. The white circles highlight areas with termination geometries caused by factors other than stratigraphic terminations and/or tectonics. (For interpretation of the references to colour in this figure legend, the reader is referred to the Web version of this article.)

younger and relatively horizontal layer due to depositional processes, whereas the orange arrow is an angular truncation caused by post-depositional erosion. When the classification window is viewed, these two different types of stratigraphic termination are hard to distinguish even by experienced seismic interpreters. By focusing our objective on reflection geometry (not stratigraphic termination type) and training a binary classifier (Contains termination or No termination), our model highlights both cases in Fig. 1- box (A) as seismic reflection terminations.

The proposed deep learning binary classification method for seismic reflection terminations identification offers an alternative to traditional mathematical approaches. Existing methods, such as those by Bugge et al. (2018) measuring reflection orientation changes, van Hoek et al. (2010) analysing seismic dip field convergence/divergence, and Wu and Hale (2015, 2016) comparing seismic normal vector fields, rely on explicit mathematical formulations of seismic attributes. Lou et al. (2024) is another deep learning approach. However, it uses a dip-based model derived from seismic as label with fewer training instances and bigger deep learning architecture. In contrast, our deep learning approach employs geological modelling with a streamlined architecture trained on extensive synthetic data. While conventional methods require manual parameters engineering (e.g., computing vector field differences or convergence metrics), the deep learning framework automatically learns discriminative patterns from seismic inputs. The proposed approach demonstrates comparable accuracy to mathematical methods with minimal human intervention and more resilience to noisy data.

While SRT-Ai achieved high performance in highlighting seismic reflection terminations, its interpretability remains limited compared to classical seismic attributes. Traditional mathematical attributes produce outputs that are directly tied to known geometric or geophysical features, making them easier to interpret in a geologic context. In contrast, the deep learning approach functions as a data-driven model, with internal representations that are not explicitly linked to predefined seismic characteristics. Despite this limitation, the model's ability to learn complex spatial patterns from labelled examples enables it to detect features that may be missed or poorly resolved by conventional attributes, often in a faster and more consistent manner.

The second challenge concerns the impact on the prediction outcome of the window size. For example, without viewing a larger portion of the data and depending on the resolution of the seismic data, the set of layers in Fig. 1-box (B) can be interpreted as downlap terminations or tilted conformable layers. To explore this issue, we consider the impact of different window sizes on the performance of SRT-Ai. Compared to all the tested seismic window sizes (Fig. 9), the original size (Fig. 9-A) highlights most of the toplaps and downlaps in the clinoforms as well as the truncation surface and the tilted layers below it. It also highlights major faults and some onlaps. On the other hand, in the double sized seismic section (Fig. 9-B) the regions of high termination probability are more compacted and smaller, mainly due to the small geological features and relatively smaller window. The CNN model does not predict much from the stretched section as most of the geological features are distorted and flattened (Fig. 9-C). The squeezed section has most of the features highlighted with an excellent prediction for the clinoforms succession and unconformity angular truncations. However, it also amplifies a lot of the noises and highlights them as terminations (Fig. 9-D). Thus, we opted for a weighted average approach grouping the

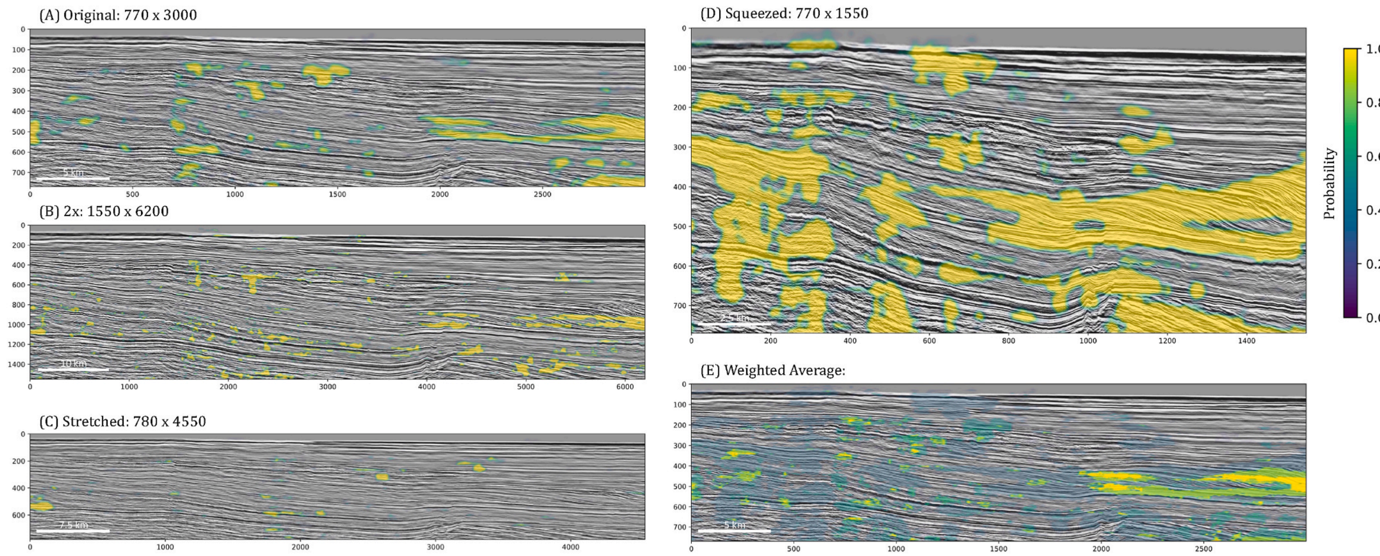

Fig. 9. The "Contains Termination" class predictions from the same seismic section image with four different sizes: (A) original size. (B) the original seismic section scaled by a factor of ~2 in both axes. (C) stretched size with increasing the x-axis only of the original seismic section. (D) squeezed size with increasing the y-axis only of the original seismic section. (E) weighted average. The weighted average yields a comprehensive approach combining the benefits from the different sizes with wider probability range.

original (50 %), squeezed (35 %), and doubled (15 %) window sizes with their different assigned weights. The choice of weights was an empirical decision based on the qualitative assessment of the performance with each window size. This nested approach offers the best of all approaches: the original size gives a focused probability highlight, the doubled window amplifies precise and smaller features, whereas the squeezed section gives a good regional guide.

The presented binary seismic reflection termination analysis provides a transitional foundation for robust multiclass frameworks. Discrete classes for specific termination types (e.g., onlap, truncation) and fadeout scenarios improve geological specificity. Future work may include integrating regional contextual prompts (e.g., information on basin evolution) with seismic attributes (amplitude variance, dip coherence) to reduce ambiguities where termination geometries overlap. Hybrid models combining stratigraphic context (sequence boundaries, depositional trends) and attribute analysis can also mitigate noise from non-stratigraphic causes. Synthetic training datasets, generated via process-based forward stratigraphic modelling and more sophisticated seismic modelling, may enhance model resilience to geometric ambiguities. While multiclass systems demand expanded labelled datasets and computational resources, their ability to reflect geological complexity justifies adoption. Future work should focus on multiclass and multilabel data classification and segmentation. By embracing multiclass frameworks, seismic interpretation can advance beyond binary paradigms, enabling more accurate stratigraphic analysis in complex systems.

The third challenge was to deal with terminations caused by reasons other than stratigraphic/tectonic regional controls. Stratigraphic terminations are not the only source of reflection terminations in seismic data. Other geophysical acquisition and processing factors such as dead traces, frequency variation, and data quality as well as lateral change in acoustic properties can cause termination geometries. From a geophysical standpoint, there are several scenarios where a reflection will diminish (fadeout) due to seismic resolution limitations or lateral changes in properties. This fadeout scenario will geometrically resemble a lateral reflection termination in seismic data. Since the objective of this study is to highlight the seismic reflection terminations associated with stratigraphic boundaries (i.e. truncation, toplap, onlap, and downlap), an additional set of data was generated using "fadeout" configuration parameters. This additional set of models generated to resemble reflections fadeouts (Fig. 6-C) and were grouped with the "No Termination" class. Although, this helped in minimizing the highlight of lateral amplitude changes as terminations, it did not eliminate it completely. Some examples of isolated areas with amplitude fadeout at smaller scales (given the appearance of a reflection termination) were still highlighted as terminations in the probability map (Fig. 8-C, white circles).

4.2. Analysis of prediction errors on test sets

Most of the mis-predicted examples in our synthetic test set were due to the low acoustic impedance contrast erasing the presence of the feature of interest in the synthetic models (e.g. Fig. 10-A, 10-B, and 10-D). Since a function was used to randomize acoustic impedance per layer, there was a probability of having two adjacent layers with very close acoustic impedance values at the termination point, effectively rendering the termination invisible in the synthetic seismic images (even though there is a termination present in the geological model). In terms of the geophysics response, this means that the reflection coefficient is almost zero at the interface. However, these are rare instances with only 13 examples out of 15 930 test cases. Despite these instances lowering the quantitative performance score of the CNN model, they were labelled based on their geological models and kept in the data to minimise our intervention in the labelling process.

On the other hand, sometimes clear truncation examples are predicted as "No Termination" (Fig. 10-C). One of the possible explanations for this is the location of the termination points. The strong termination in this example (Fig. 10-C) is at the edge of the window which makes the amplitude of the weaker terminated reflections on top of it a major factor in mis-predicting the termination. Although it is clear in all the examples that reflections are terminating at both sides of each window, this should not be classified as seismic reflection terminations as only reflections terminating within the window against another reflection truly characterise the "Contains Termination" class. This is often more complicated with real seismic data.

Though it is hard to understand and pin-point exactly the reasons for the mis-predictions in real seismic data, there is some evidence that points to potential causes. If we try to summarize the possible reasons for these mis-predictions, they fall within one of three scenarios: (1) Conformable continuous layers "No Termination" dominating most of

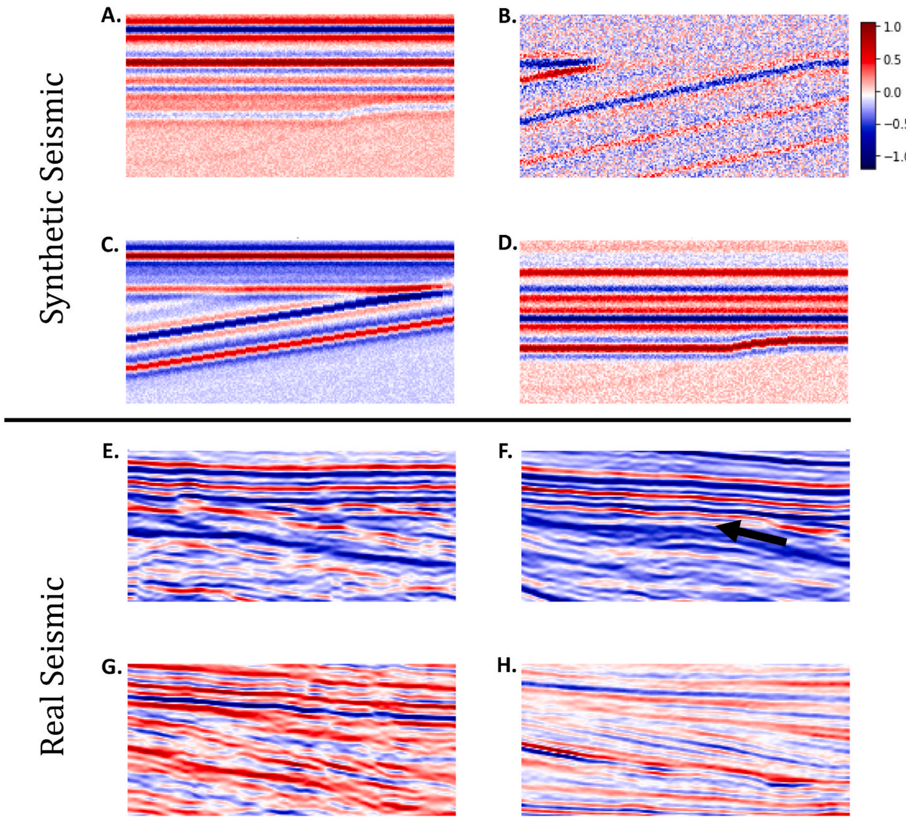

Fig. 10. Examples from incorrect predictions. Both the real and the synthetic examples are from "Contains Termination" class and predicted as "No Termination class". While the dashed line indicates the termination surface, the arrows show the direction of terminations with the termination point at the tip of the arrows.

the window (Fig. 10-F); (2) A big difference in amplitude between the conformable "No Termination" and the terminated "Contains Termination" layers (Fig. 10-E and 10-F); and (3) Seismic resolution at the termination point (Fig. 10-G and 10-H). The resolution and quality of the real seismic data will always be a major challenge in enhancing the model's predictions.

4.3. Interpretation versus observation

Humans are limited to their senses and what can be observed visually. Shadows, colours, and perspective may affect our observations. On the other hand, previous experiences, educational background, and emotional state can influence our interpretation and decisions. Most of the geoscience questions, especially those related to characterization and modelling, do not necessarily have a straightforward solutions or definite right answer (Bond et al., 2011). Evaluating probabilities and close to reality scenarios requires knowledge, experience, technical skills, and imagination. We believe, artificial intelligence and machine learning can play a major role in guiding our interpretation and decisions making process. Tools like the one presented can guide geoscientist's initial screening of any new seismic dataset without forcing a specific geological model or interpretation. The final interpretation, modelling, and decision making will remain in the hands of engineers and geoscientists.

The SRT-Ai tool can highlight clinoforms and unconformities with their associated toplaps, downlaps, and angular truncations (Fig. 8). When we compare the highlighted probability with the interpretation arrows in Fig. 8-C, we observe a large overlap. These arrows are based on human interpretation and subjected to interpretation bias. However, we view our tool as an AI guide that highlights major features to help geoscientists start their seismic interpretation from a consistent base ground. SRT-Ai can also help junior interpreters start their interpretation and build their confidence. Bond et al. (2011) observed that people with the least seismic experience hesitated for the longest in starting the interpretation exercise. Having a stratigraphic pretrained model that can highlight major stratigraphic features early in the seismic interpretation workflow should minimise the challenge of starting the interpretation.

Areas that are highlighted by SRT-Ai are not limited to clinoforms and unconformity surfaces, faults and debris flows have been also observed and detected as regions showing reflection terminations (Fig. 8-C). These are geological features that we did not explicitly train the CNN model to recognize, but that show seismic reflection termination geometries where reflections terminate against other reflections. The model was able to observe and highlight them to guide the eye of the interpreter to them as features of potential interest requiring closer human examination.

SRT-Ai can be used as an observation tool to highlight seismic reflection terminations at an early stage in the interpretation and before starting any horizon and/or fault picking. The aim of the attribute is to help interpreters to quickly 'get their eye-in' to where the key seismic stratigraphic boundaries are.

5. Conclusions

The quantitative and qualitative analysis of SRT-Ai predictions show promising results: 91 % accuracy and 96 % precision scores on real seismic images is a milestone toward automating the identification of seismic reflection terminations. Using synthetic seismic dataset to train a deep learning model on predicting seismic reflection terminations was proven to be an efficient approach. It solves the problem of lacking enough labelled data, reduces the human interpretation bias, and eliminates the need for manual labelling. Having general, complex, diverse, and big labelled training datasets was a crucial step in the success of this study.

Deep learning can be a powerful and transformative tool in geosciences applications, especially seismic interpretation. The proposed attribute is an example of automating the process of identifying seismic reflection terminations making it fast and more efficient. This tool will assess seismic interpreter by highlighting seismic reflection termination at an early stage of seismic data scanning. Integrating SRT-Ai in seismic interpretation workflows will minimise uncertainties, expedite seismic reconnaissance process, and reduce the dependence on human visual assessments.

CRediT authorship contribution statement

Waleed M. AlGharbi: Writing – original draft, Methodology, Formal analysis, Data curation, Conceptualization. **Rebecca E. Bell:** Writing – review & editing, Supervision. **Cédric M. John:** Writing – review & editing, Supervision.

Authorship contribution statement

Waleed AlGharbi: main researcher, developed the code, performed the analyses, and wrote the paper. Rebecca E. Bell: supervised the geophysical part of the project, reviewed, and edited the paper. Cédric M. John: Project PI, supervised the machine learning part of the project, reviewed, and edited the paper.

Code availability section

Name of the code/library: Seismic Reflection Termination Attribute (SRT-Ai).

Contact: w.algharbi21@imperial.ac.uk.

Hardware requirements: The operating system used was Ubuntu Linux release 22.04 on an Intel Xeon processor, 128 GB (4 × 32GB) RAM, and NVIDIA Quadro RTX 8000 GPU.

Program language: Python.

Software required: The data generation, Convolutional Neural Networks (CNN) training, testing, and evaluation were done using Python (version 3.10.6) (Van Rossum and Drake Jr, 1995). A number of external dependencies (Python libraries) were used: TensorFlow (2.9.1) (Abadi et al., 2016), TensorFlow-keras (2.9.0) (Chollet, 2015), NumPy (1.21.5) (Harris et al., 2020), bruges (0.5.4) (Hall et al., 2022), SEGY-SAK (0.3.4) (Hallam et al., 2024), SciPy (1.8.0) (Virtanen et al., 2020), Scikit-learn (0.23.2) (Pedregosa et al., 2011), Matplotlib (3.5.1) (Hunter, 2007), and seaborn (0.12.0) (Waskom, 2021).

Program size: 30 MB.

The source codes are available for downloading at the link: https://github.com/wa314/SRT-Ai and https://doi.org/10.5281/zenodo.15914897.

Declaration of competing interest

The authors declare the following financial interests/personal relationships which may be considered as potential competing interests: Waleed AlGharbi reports financial support was provided by Saudi Arabian Oil Co. If there are other authors, they declare that they have no known competing financial interests or personal relationships that could have appeared to influence the work reported in this paper.

Acknowledgments

The results presented here are part of W.M. AlGharbi's PhD research at Imperial College London, funded by Saudi Aramco. We thank Geoscience Australia for the publicly available seismic data. We would like also to thank John Lab at Queen Mary University of London and the Landscapes and Basins Research Group at Imperial College London, specifically Zayad AlZayer, for their valuable contributions and insightful discussions during the various stages of preparing this work.

Appendix A. Predictions on real seismic

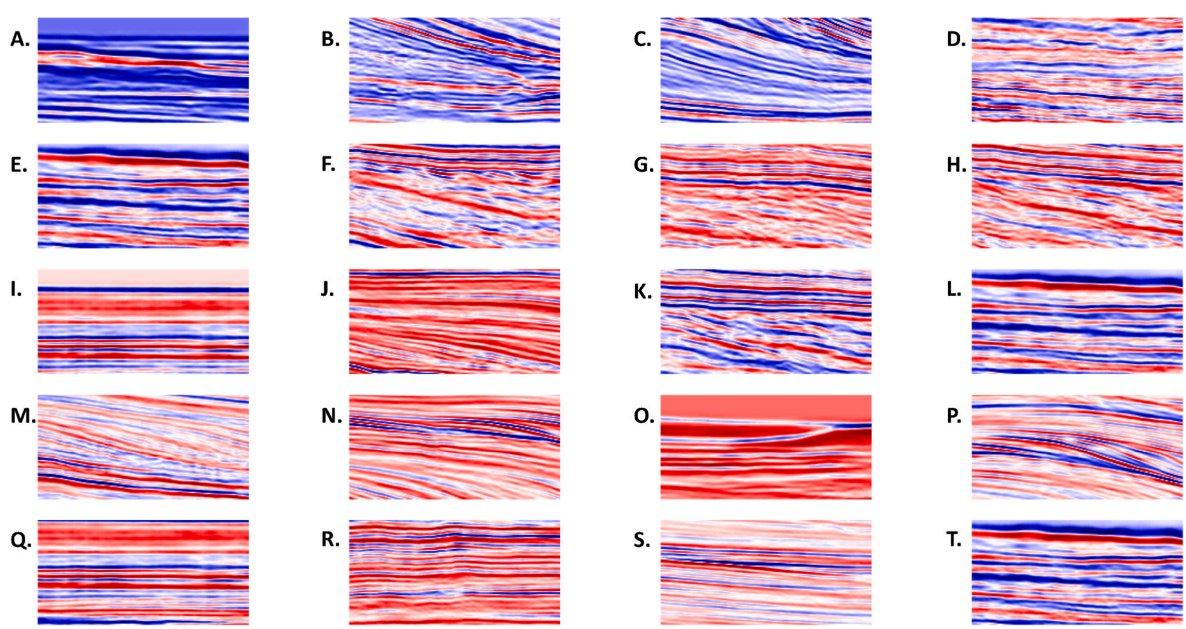

Fig. A.1. Sliced examples from the real seismic survey, Demeter NW Australia. These examples were used to test the performance of SRT-Ai on real seismic. Slicing and labelling these windows requires a regional understanding of the basin and its geological setting. Each window should have only one feature. However, we expect conformable continuous layers to be part of all windows. Faults and noise may affect the continuity of the conformable examples. Figure A.1-R shows a fault without a big displacement that affects the flatness of the layers. The truncations in Figures (A.1-F, G, H & K) are clear terminations of strata at erosional surfaces. Although we were able to differentiate between figures (A.1-J "toplap") and (A.1-K or H "truncation) analysing the regional geology of the basin, it is still difficult for human eyes even experienced once to differentiate using theses windows only.

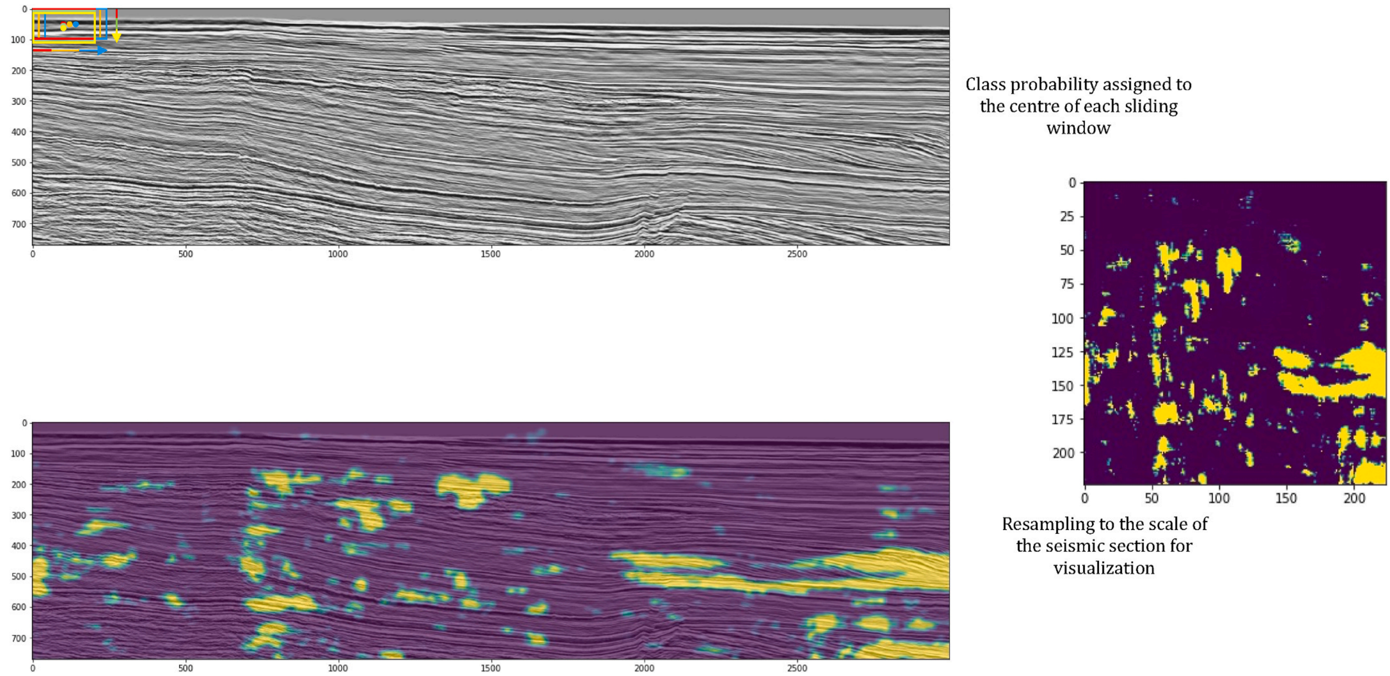

Fig. A.2. A custom function was used to extract patches and predict their class probability with a fixed window size of (200 pixels × 99 pixels), sliding in a horizontal stride of ten and a vertical stride of three. The coloured windows in the top left corner of the seismic section show examples of different patches and the location of the prediction at the centre.

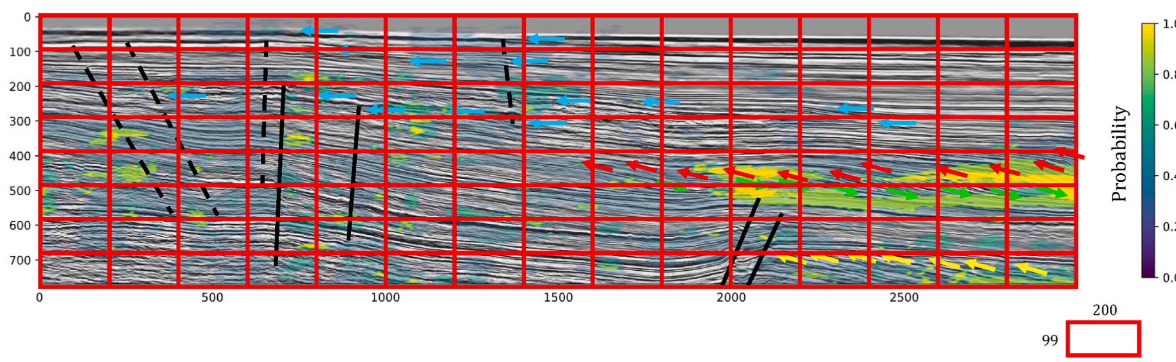

Fig. A.3. Quantifying the model performance by patching the seismic section into (200 x 99) windows and compare the manual labels with the model predictions in each window, applying 0.6 probability threshold.

$$Accuracy = \frac{TP + TN}{TP + TN + FP + FN} = \frac{42 + 51}{42 + 51 + 12 + 15} = 0.775$$

$$Precision = \frac{TP}{TP + FP} = \frac{42}{42 + 12} = 0.778$$

$$Recall = \frac{TP}{TP + FN} = \frac{42}{42 + 15} = 0.737$$

$$F1\ Score = \frac{TP}{TP + \frac{1}{2}(FP + FN)} = \frac{42}{42 + \frac{1}{2}(12 + 15)} = 0.757$$

Data availability

Data will be made available on request.

References

Abadi, M., Barham, P., Chen, J., Chen, Z., Davis, A., Dean, J., Devin, M., Ghemawat, S., Irving, G., Isard, M., Kudlur, M., 2016. TensorFlow: a system for Large-Scale machine learning. In: 12th USENIX Symposium on Operating Systems Design and Implementation (OSDI 16), pp. 265–283.

Anell, I., Wallace, M.W., 2020. A fine balance: accommodation dominated control of contemporaneous cool-carbonate shelf-edge clinoforms and tropical reef-margin trajectories, North Carnarvon Basin, Northwestern Australia. Sedimentology 67 (1), 96–117.

Bennett, K.J., Bussell, M.R., 2006. Demeter high resolution 3D seismic survey – revitalised development and exploration on the northwest shelf, Australia. The APPEA Journal 46 (1), 101–126.

Bond, C.E., Philo, C., Shipton, Z.K., 2011. When There isn't a Right Answer: interpretation and reasoning, key skills for twenty-first century geoscience. Int. J. Sci. Educ. 33 (5), 629–652.

Bugge, A.J., Clark, S.R., Lie, J.E., Faleide, J.I., 2018. A case study on semiautomatic seismic interpretation of unconformities and faults in the southwestern Barents Sea. Interpretation 6 (2), SD29–SD40.
Catuneanu, O., Abreu, V., Bhattacharya, J.P., Blum, M.D., Dalrymple, R.W., Eriksson, P. G., Fielding, C.R., Fisher, W.L., Galloway, W.E., Gibling, M.R., Giles, K.A., 2009. Towards the standardization of sequence stratigraphy. Earth Sci. Rev. 92 (1–2), 1–33.
Chollet, F., 2015. Keras. Available at: https://github.com/fchollet/keras.
Chopra, S., Marfurt, K.J., 2012. Evolution of seismic interpretation during the last three decades. Lead. Edge 31 (6), 654–676.
Christie-Blick, N., Mountain, G.S., Miller, K.G., 1990. Seismic stratigraphic record of sea-level change. Sea-level change. National Academy of Sciences Studies in Geophysics. National Academy Press, Washington, D.C., pp. 116–140
Di, H., Wang, Z., AlRegib, G., 2018. Why using CNN for seismic interpretation? An investigation. In: SEG International Exposition and Annual Meeting. Anaheim, California, USA.
Dragoset, B., 2005. A historical reflection on reflections. Lead. Edge 24 (Supplement), S46–S71.
Eberli, G.P., Anselmetti, F.S., Kroon, D., Sato, T., Wright, J.D., 2002. The chronostratigraphic significance of seismic reflections along the Bahamas Transect. Mar. Geol. 185 (1–2), 1–17.
Gao, H., Wu, X., Zhang, J., Sun, X., Bi, Z., 2023. ClinoformNet-1.0: stratigraphic forward modeling and deep learning for seismic clinoform delineation. Geosci. Model Dev. Discuss. (GMDD) 2023, 1–29.
Geoscience Australia, 2023. Regional Geology of the Northern Carnarvon Basin. Australian Government. https://www.ga.gov.au/scientific-topics/energy/province-sedimentary-basin-geology/petroleum/acreagerelease/northerncarnarvon.
Géron, A., 2019. Hands-on Machine Learning with Scikit-Learn, Keras, and TensorFlow. O'Reilly Media, Inc.
Gholamy, A., Kreinovich, V., 2014. Why Ricker wavelets are successful in processing seismic data: towards a theoretical explanation. In: 2014 IEEE Symposium on Computational Intelligence for Engineering Solutions (CIES). IEEE, pp. 11–16.
Gold, D., Heinemann, N., Porjesz, R., Bolton, R., Rhodes, G., Roy, P., Bunker, E., Booth, M., 2022. How a multidisciplinary, data-driven geoscience approach is required to help achieve the energy transition goals. First Break 40 (10), 51–57.
Gregory, A.R., 1977. Aspects of rock physics from laboratory and log data that are important to seismic interpretation: section 1. Fundamentals of stratigraphic interpretation of seismic data. In: Payton, C.E. (Ed.), Seismic Stratigraphy-Applications to Hydrocarbon Exploration. American Association of Petroleum Geologists.
Gu, X., Lu, W., Ao, Y., Li, Y., Song, C., 2023. Seismic stratigraphic interpretation based on deep active learning. IEEE Trans. Geosci. Rem. Sens. 61, 1–11.
Hall, M., Bianco, E., Bougher, B., Dramsch, J., Amato del Monte, A., Niccoli, M., Bentley, M., Kazei, V., Martin, T., Favela, V., Uieda, L., 2022. Bruges. GitHub. https://github.com/agilescientific/bruges.
Hallam, T., Scott, R., Dinneen, C., Amato del Monte, A., Sanger, W., Purves, S., 2024. SEGY-SAK. GitHub. https://github.com/trhallam/segysak.
Han, C., Cader, A., Brownless, M., 2021. Subsurface seismic interpretation technologies and workflows in the energy transition. First Break 39 (10), 85–93.
Harris, C.R., Millman, K.J., Van Der Walt, S.J., Gommers, R., Virtanen, P., Cournapeau, D., Wieser, E., Taylor, J., Berg, S., Smith, N.J., Kern, R., 2020. Array programming with NumPy. Nature 585 (7825), 357–362.
Hart, B., Chen, M.A., 2004. Understanding seismic attributes through forward modeling. Lead. Edge 23 (9), 834–841.
Hull, J., Griffiths, C., 2002. Sequence stratigraphic evolution of the Albian to recent section of the Dampier Sub-basin, North West Shelf, Australia. In: Keep, M., Moss, S. (Eds.), The Sedimentary Basins of Western Australia 3: Proceedings of the Petroleum Exploration Society of Australia Symposium. PESA, Perth, WA, pp. 617–639.
Hunter, J.D., 2007. Matplotlib: a 2D graphics environment. Comput. Sci. Eng. 9 (3), 90–95.
Kaur, H., Pham, N., Fomel, S., Geng, Z., Decker, L., Gremillion, B., Jervis, M., Abma, R., Gao, S., 2023. A deep learning framework for seismic facies classification. Interpretation 11 (1), T107–T116.
Kearey, P., Brooks, M., Hill, I., 2002. An Introduction to Geophysical Exploration, 4. John Wiley & Sons.
Krebes, E.S., 2004. Seismic forward modeling. CSEG Recorder 30, 28–39.
LeCun, Y., Bottou, L., Bengio, Y., Haffner, P., 1998. Gradient-based learning applied to document recognition. Proc. IEEE 86 (11), 2278–2324.
Lou, Y., Zhang, X., Liu, N., Chen, Y., Zheng, J., 2024. Seismic unconformity estimation via ECA-UNet++ with physical knowledge constrained synthetic data. IEEE Trans. Geosci. Remote Sens. 62, 1–14.
Nair, V., Hinton, G.E., 2010. Rectified linear units improve restricted Boltzmann machines. In: Proceedings of the 27th International Conference on Machine Learning. ICML-10), pp. 807–814.
Pedregosa, F., Varoquaux, G., Gramfort, A., Michel, V., Thirion, B., Grisel, O., Blondel, M., Prettenhofer, P., Weiss, R., Dubourg, V., Vanderplas, J., 2011. Scikit-learn: machine learning in Python. J. Mach. Learn. Res. 12, 2825–2830.
Posamentier, H.W., Paumard, V., Lang, S.C., 2022. Principles of seismic stratigraphy and seismic geomorphology I: extracting geologic insights from seismic data. Earth Sci. Rev. 228, 103963.
Riding, J.B., Rochelle, C.A., 2009. Subsurface characterization and geological monitoring of the CO2 injection operation at Weyburn, Saskatchewan, Canada. Geol. Soc. London Spec. Publ. 313 (1), 227–256.
Ricker, N., 1953. The form and laws of propagation of seismic wavelets. Geophysics 18 (1), 10–40.
Russell, B.H., 1988. Introduction to seismic inversion methods (No. 2). Society of Exploration Geophysicists Books.
Scherer, D., Müller, A., Behnke, S., 2010. Evaluation of pooling operations in convolutional architectures for object recognition. In: Diamantaras, K., Duch, W., Iliadis, L.S. (Eds.), Artificial Neural Networks – ICANN 2010. ICANN 2010. Lecture Notes in Computer Science, 6354. Springer, Berlin, Heidelberg.
Srivastava, N., Hinton, G., Krizhevsky, A., Sutskever, I., Salakhutdinov, R., 2014. Dropout: a simple way to prevent neural networks from overfitting. J. Mach. Learn. Res. 15 (1), 1929–1958.
Summerhayes, C.P., 1986. Sealevel curves based on seismic stratigraphy: their chronostratigraphic significance. Palaeogeogr. Palaeoclimatol. Palaeoecol. 57 (1), 27–41.
Telford, W.M., Geldart, L.P., Sheriff, R.E., 1990. Applied Geophysics, second ed. Cambridge University Press, Cambridge.
Tschannen, V., Delescluse, M., Ettrich, N., Keuper, J., 2020. Extracting horizon surfaces from 3D seismic data using deep learning. Geophysics 85 (3), N17–N26.
Vail, P.R., Mitchum Jr, R.M., 1977. Seismic Stratigraphy and Global Changes of Sea Level, Part 1: Overview. Seismic Stratigraphy-Applications to Hydrocarbon Exploration, Charles E. Payton.
Vail, P.R., Mitchum Jr, R.M., Thompson, I.I.I.S., 1977. Seismic Stratigraphy and Global Changes of Sea Level, Part 3: Relative Changes of Sea Level from Coastal Onlap. Seismic Stratigraphy-Applications to Hydrocarbon Exploration, Charles E. Payton.
van Hoek, T., Gesbert, S., Pickens, J., 2010. Geometric attributes for seismic stratigraphic interpretation. Lead. Edge 29 (9), 1056–1065.
Van Rossum, G., Drake Jr, F.L., 1995. Python reference manual, Centrum voor Wiskunde en Informatica Amsterdam.
Virtanen, P., Gommers, R., Oliphant, T.E., Haberland, M., Reddy, T., Cournapeau, D., Burovski, E., Peterson, P., Weckesser, W., Bright, J., Van Der Walt, S.J., 2020. SciPy 1.0: fundamental algorithms for scientific computing in Python. Nat. Methods 17 (3), 261–272.
Vizeu, F., Zambrini, J., Tertois, A.L., da Graça e Costa, B.D.A., Fernandes, A.Q., Canning, A., 2022. Synthetic seismic data generation for automated AI-based procedures with an example application to high-resolution interpretation. Lead. Edge 41 (6), 392–399.
Waldeland, A.U., Jensen, A.C., Gelius, L.J., Solberg, A.H.S., 2018. Convolutional neural networks for automated seismic interpretation. Lead. Edge 37 (7), 529–537.
Waskom, M.L., 2021. Seaborn: statistical data visualization. J. Open Source Softw. 6 (60), 3021.
Wrona, T., Pan, I., Bell, R.E., Gawthorpe, R.L., Fossen, H., Brune, S., 2021. 3D seismic interpretation with deep learning: a brief introduction. Lead. Edge 40 (7), 524–532.
Wu, X., Geng, Z., Shi, Y., Pham, N., Fomel, S., Caumon, G., 2020. Building realistic structure models to train convolutional neural networks for seismic structural interpretation. Geophysics 85 (4), WA27–WA39.
Wu, X., Hale, D., 2015. 3D seismic image processing for unconformities. Geophysics 80 (2), IM35–IM44.
Wu, X., Hale, D., 2016. Automatically interpreting all faults, unconformities, and horizons from 3D seismic images. Interpretation 4 (2), T227–T237.
Zhang, G., Wang, Z., Chen, Y., 2018. Deep learning for seismic lithology prediction. Geophys. J. Int. 215 (2), 1368–1387.
Zheng, Y., Zhang, Q., Yusifov, A., Shi, Y., 2019. Applications of supervised deep learning for seismic interpretation and inversion. Lead. Edge 38 (7), 526–533.